The Role of Carbonaceous Fragments on the Functionalization and Electrochemistry of Carbon Materials

Rui Gusmão,[a,b] Eunice Cunha,[a] Conceição Paiva,[a] Dulce Geraldo,[b] Fernanda Proença,[b] Fátima Bento[b]

[a]   Dr. R. Gusmão, Eunice Cunha, Dr M.C. Paiva
Instituto de Polímeros e Compósitos/I3N, Universidade do Minho, Campus de Azurem, 4800-058 Guimarães (Portugal)
[b]   Dr. M. D. Geraldo, Dr. M. F. Bento, Prof. M. F. Proença
Centro de Química, Universidade do Minho, Campus de Gualtar, 4710-057 Braga (Portugal)

Abstract

Carbonaceous fragments (CF) formed by acid treatment of carbon materials have important properties that are not completely understood. In this work, CF were produced by oxidation of CNT using mineral acid followed by treatment with NaOH. The role of CF on CNT voltammetric properties was studied using different materials: oxidized CNT (a-CNT), a-CNT refluxed in NaOH and neutralized with HCl (b-CNT), pristine CNT exposed to a CF suspension (c-CNT), and b-CNT exposed to a CF suspension (r-CNT). The extension of functionalization of these materials was evaluated by TGA. The spectroscopic characterization (UV/Vis, fluorescence, FTIR, Raman and NMR) of CF indicates the presence of graphene-type conjugated aromatic rings with highly oxidized moieties.

In this work we demonstrate that CF are responsible for the ameliorated voltammetric properties of oxidized CNT. Adsorption of CF on oxidized and non-oxidized CNT showed that CF provide active sites for hydroquinone (HQ) adsorption, enhancing current responses. The interaction of CF with carbon materials depended on both the surface oxidation degree and the surface roughness. Voltammograms from CF adsorbed on oxidized CNT indicate the presence of labile supramolecular structures with a voltammetric response typical of quinoid units. Carbon materials functionalized with CF displayed lower peak potentials and higher currents (30 to 180 %) than the un-modified electrodes demonstrating that CF is a promising material for sensors design.

1. Introduction

Recurrent use of carbon nanoparticles (CNP) in sensors design is due to their unique features that change dramatically the interface properties of electrodes.[1,2] Improvement of heterogeneous charge transfer rates and increased ability to immobilize molecules may justify the ameliorated sensitivity and detection limits achieved with CNP modified electrodes.[3,4] The high surface area,[5] the increased amount of edges-plane sites[6] and the presence of catalytic impurities are often indicated as key features for CNP electrochemical properties. The effect of impurities, either metallic,[7] graphitic[8–14] or of residual surfactants[15] has been studied on the catalytic and redox properties of CNP.

Purification of CNP may be extremely challenging since the impurities, particularly graphitic, display similar chemical properties. Oxidation by strong oxidizing agents under reflux,[16–18] electrochemical oxidation[19–21] or by heat[22] are alternative treatments for CNP. The introduction of oxygen groups in the graphitic impurities improves their solubility in polar solvents and allows their removal from the CNP surface. These oxidative treatments have drawbacks, namely their limited efficiency on removing impurities,[23] the production of structural defects and the extensive functionalization of CNP.[20,24,25] Graphene oxide (GO)[26]

1

and highly oxidized carbonaceous fragments (CF), also denominated as carbonaceous debris (OD),[27] are important products that result from oxidative treatments of CNP.[17,18] Regardless of the starting carbon material undergoing oxidation, CF are generally described as highly oxidized polyaromatic fragments strongly adsorbed on the carbon matrix by π-π stacking, hydrogen bonding, and van der Waals interactions.[28] These nanostructures may be extracted from the precursor materials by reflux in NaOH solution.[29–32]

Several authors studied the effect of CF on the electrochemical performance of CNT and graphene materials. [32–39] The presence of CF was reported to have a positive effect on the electrochemical oxidation of β-nicotinamide adenine dinucleotide (NADH) and ascorbic acid (AA) at glassy carbon electrode coated with CNT.[32] Conversely, the oxidation of NADH mediated by 1,10-phenantroline-5,6-dione was adversely influenced by the presence of CF on the GO surface.[33] The presence of CF on the surface of GO limits the oxidation of dopamine (DA),[30] while on the surface of reduced graphene (RG) CF favors the oxidation of DA,[34] AA, NADH, aminophenol and H_2O_2.[35] Besides faradaic processes, the capacitive performance of carbon materials can be highly influenced by the presence of CF on their surface.[36,37] The removal of CF produced a significant decrease of the capacitance of graphene, while their re-adsorption produced a capacitance recovery. A possible explanation for the improved conductivity of graphene samples containing CF is the increased wettability of the material. As a consequence the restacking of graphene sheets may be hindered, increasing the exposed surface area. [36]

The chemical nature of the CF is not entirely known. More than one hundred compounds were detected by ESI FT-ICR MS in CNT oxidation debris.[40] Several methods were applied to characterize this material in terms of structure and electrochemical performance. Thermogravimetric analysis (TGA), reported their decomposition to take place above 200 ºC.[33] Scanning transmission X-ray microscopy-related techniques were applied to characterize oxidized CF on CNT, demonstrating the presence of a heavily oxidized CF coating.[41] A structure consisting of "three or more fused benzene rings with extended oxygen containing functional groups" was suggested by the fluorescence spectrum,[32] and supported by Fourier Transform Infrared Spectroscopy (FTIR) and X-ray photoelectron spectroscopy (XPS) analysis. [32,35]

In the present work, the CF produced by treatment of the CNT with concentrated HNO_3 were characterized by thermal analysis (TGA) and spectroscopic techniques (UV/Vis, fluorescence, FTIR, Raman, NMR and EDS). These CF were used to modify electrodes of different carbon materials. Hydroquinone (HQ) was used a molecular probe for the detection of carbonyl and hydroxyl groups at the surface of CNT modified electrode[22] and as a model polyphenol. Polyphenols have natural occurrence and can exhibit cytotoxic activity[42] or act as antioxidants.[43] Besides, synthetic polyphenols used as textile dyes are frequently discarded as residues.[44] The development of sensors for this class of compounds is therefore of great importance to health, food and environmental applications.

2. Experimental Part

Materials

Multiwall carbon nanotubes (CNT, NC7000, purity > 90 %, average length of 1.5 μm, average diameter of 9.5 nm) were purchased from Nanocyl, S.A. (Belgium) and employed throughout. Pyrograph® III carbon

nanofibers (CNF, PR-24-PS, hollow fibers with wide diameter range from 60 to 150 nm, maximum length 100 μm) were acquired from Applied Sciences, Inc. (USA). Graphite powder ($G_{1μm}$, 1-2 μm) was purchased from Aldrich. Hydroquinone (HQ, Riedel-de Haen) and all other chemicals were of analytical grade or higher and were used as received. Milli-Q water was used in the preparation of solutions.

Instrumentation

Infrared spectra of CF were recorded on an ABB FTIR–FTLA2000 analyzer within the range of 500 - 4000 cm^{-1} using KBr pellets (about 2 mg of material in 98 mg of KBr). The UV/Vis spectra of CF aqueous suspensions were recorded on a Shimadzu UV-2501 model. The absorption measurements were carried out in a quartz cell with a path length of 1 cm. Fluorescence spectra of CF suspensions were obtained at room temperature on a FluoroMax-4 spectrophotometer (Horiba) using a quartz cell with a path length of 1 cm and a slit width of 5 nm. The excitation wavelength was set at the maximum peak wavelength (290 nm) of the absorption spectra of CF suspension obtained from CNT oxidized during 6 h (CF_{6h}).

Raman spectra were acquired on a Horiba LabRam HR Evolution confocal microscope using a 532 nm (2.33 eV) excitation laser. A 100x objective lens was used to focus the laser light on the sample. The samples were prepared by spraying the CF suspension onto a glass slide and drying.

The NMR spectra were recorded on a Bruker Avance 3400 at 400 MHz for ^{1}H and 100 MHz for ^{13}C, including DEPT 135. Deuterated water was used as solvent. The chemical shifts are expressed in δ (ppm).

A Modulated Thermogravimetric Analyzer Q500 (TA Instruments) was used in dynamic mode for the CNT characterization. The samples were heated from room temperature to 800 °C at 10 °C min^{-1} under a constant nitrogen flow of 60 mL min^{-1}.

Scanning transmission electron microscopy (STEM) was performed using a FEI Quanta 400 FEG ESEM equipped with EDAX Genesis X4M.

An Autolab PGSTAT30 potentiostat / galvanostat (Eco Chemie, The Netherlands) controlled by GPES 4.9 software was used in voltammetric experiments. A three-electrode configuration cell (v = 10 mL) was used at room temperature. A glassy carbon electrode (GCE, r = 1.5 mm, CHI104, CH Instruments, Inc.) was used as working electrode, a platinum wire as auxiliary electrode and an Ag/AgCl (3.0 M KCl, CHI111, CH Instruments, Inc.) as a reference electrode. Commercially available screen printed carbon electrodes (SPCE, DRP-110, carbon disk working electrode r = 2 mm, silver pseudo-reference electrode and carbon secondary electrode) were acquired from DropSens. Voltammetric measurements using SPCE were performed covering the three electrodes with a 50 μL drop of solution. Cyclic voltammograms were recorded at 100 mV s^{-1}.

Procedures

The CNT were subjected to the treatments illustrated in Figure 1. The as-received CNT (CNT_{prist}, 800 mg) were refluxed in concentrated HNO_3 (100 mL) at 100 - 110 ºC for 1, 3 and 6 hours. After cooling to room temperature, the CNT were centrifuged, filtered and rinsed with Milli-Q water until the filtrate showed no evidence for the presence of acid, by pH measurements. The acid-treated CNT (a-CNT) were dried in a vacuum oven (Büchi glass oven B-580) overnight at 80 ºC. Subsequently, a sample of 130 mg of a-CNT were refluxed in 0.1 M NaOH (100 mL) for 1 hour. After the mixture was cooled to room temperature, the

brownish supernatant (CF_{0h}, CF_{1h}, CF_{3h} or CF_{6h} depending on the HNO_3 refluxing time) was separated from the black precipitate. The pH of the brownish supernatant containing CF_{6h} was adjusted to 7 with 0.1 M HCl. The precipitate obtained from 6 h of HNO_3 reflux and 1 h of NaOH reflux (b-CNT) was re-suspended in water, neutralized with 0.1 M HCl, rinsed thoroughly with Milli-Q water and then dried overnight at 80 ºC under vacuum. A sample of 50 mg of b-CNT was added to 50 mL of CF_{6h} suspension and stirred for 1 hour, then filtered and rinsed with Milli-Q water. The solid (r-CNT) was then dried under vacuum. This procedure was repeated with CNT_{prist} to prepare the c-CNT. Suspensions of different CNT materials (a-CNT, b-CNT, c-CNT and r-CNT) were prepared in ethanol: water (1:1) at concentrations ranging from 1.01 to 1.08 mg mL^{-1}. CNT_{prist} suspensions (1.02 mg mL^{-1}) were prepared in n-hexane. Suspensions were initially sonicated for 5 min in an ice bath and for 30 seconds prior to use. The different suspensions drop casted on the GCE surface, were allowed to dry under a lamp. Prior to modification the GCE surface was polished with alumina (0.3 and 0.05 µm) on a polishing pad, abundantly rinsed with deionized water and dried. A fixed amount of each CNT material (4 µg) was deposited onto the GCE surface by drop casting *ca.* 4 µL of the corresponding CNT suspension to prepare CNT_{prist}@GCE, a-CNT@GCE, b-CNT@GCE c-CNT@GCE and r-CNT@GCE.

GCE modified electrodes CNF@GCE and $G_{1µm}$@GCE, containing 8 µg of CNF or of $G_{1µm}$, were prepared by drop casting *ca.* 8 µL of each suspension onto the electrode surface. The suspensions of CNF (1.31 mg mL^{-1}) and $G_{1µm}$ (1.46 mg mL^{-1}) were prepared in methanol: water (1:1). These electrodes were further modified by drop casting 10 µL of the CF_{6h} suspension (*ca.* 0.8 mg L^{-1}, evaluated by TGA data, see Results and discussion section) on the surface of: SPCE (CF@SPCE); GCE (CF@GCE); $G_{1µm}$-GCE (CF-$G_{1µm}$@GCE) and CNF-GCE (CF-CNF@GCE).

Blank solution was prepared by mixing *ca.* 13 g of potassium phosphate monobasic with 10 g of potassium phosphate dibasic and pH adjusted to 7.2 with potassium hydroxide (PB, 0.15 M). Milli-Q water was added up to a final volume of 500 mL. HQ solutions (0.50 mM) were prepared in PB.
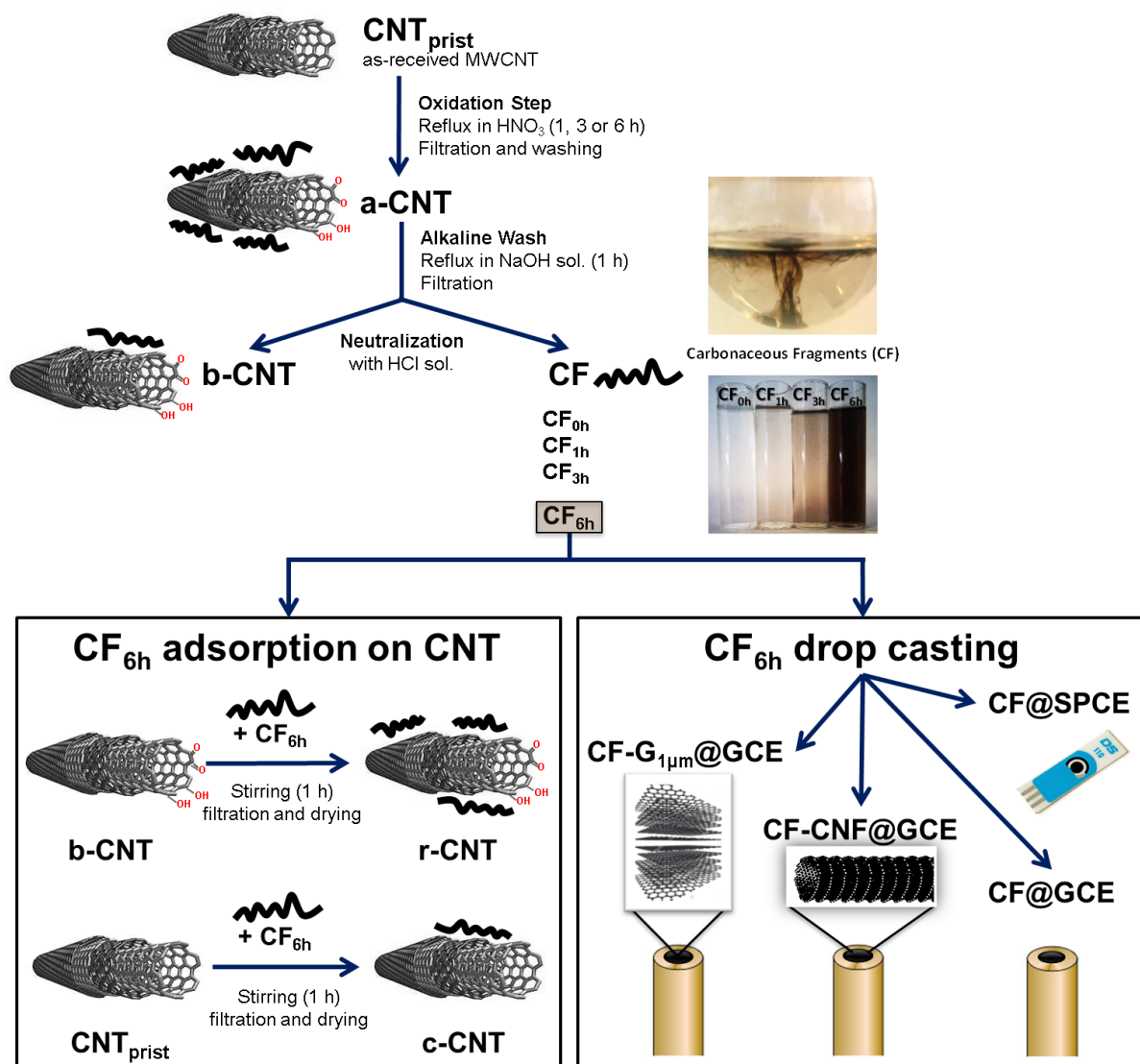
Figure 1. Schematic illustration of: the CNT treatments carried out for the preparation of carbonaceous fragments suspensions (CF); the functionalization of different CNT and of the surface of carbon electrodes with CF_{6h}. CNT_{prist}: pristine CNT; a-CNT: CNT oxidized in HNO_3 reflux; b-CNT: obtained by treatment of a-CNT with 0.1 M NaOH, 1 h of reflux; c-CNT: CNT_{prist} mechanically stirred in CF_{6h} suspension; r-CNT: b-CNT mechanically stirred in CF_{6h} suspension. CF-$G_{1\mu m}$@GCE: GCE coated with graphite powder and modified with CF_{6h}; CF-CNF@GCE: GCE coated with carbon nanofibers and modified with CF_{6h}; CF@GCE: GCE modified with CF_{6h}; CF@SPCE: SPCE modified with CF_{6h}.

The sample for NMR spectroscopy was prepared as follows. The solid sample obtained by complete removal of water from the neutralized solution of CF_{6h} in a rotary evaporator was a dark grey material containing CF_{6h} and NaCl generated in the neutralization process (*ca.* 80%). This material was partially solubilized in deuterated water (30 mg in 600 μL) and the dark grey solid that remained in suspension was filtered through fiber-glass paper. The transparent grey solution was submitted for ^{1}H and ^{13}C NMR spectroscopic analysis. The data for the ^{13}C NMR spectrum was accumulated for 67 h at 20 ºC. During this time period, some dark grey solid was deposited at the bottom of the NMR tube.

3. Results and discussion

Thermal characterization of the different CNT materials

The CNT, pristine and collected after treatment, were analyzed by thermogravimetric analysis (TGA) and the results are presented in Figure 2. The pristine CNT are stable up to 800 ºC under nitrogen (1.3 % weight loss), while the oxidized and treated CNT show a significant weight loss. This may be assigned to loss of CO and CO_2 by thermal degradation of the oxidized CNT surface. The weight loss starts above 150 ºC and continues slowly with increasing temperature, showing the thermal decomposition of a variety of oxidation products within a wide range of degradation energies. The overall weight loss at 800 ºC is greater for a-CNT (20.0 %), decreasing after alkali treatment, yielding b-CNT (13.8 %). This weight loss difference correlates with the oxidized debris that are eliminated from a-CNT surface. An increase of weight loss was observed for r-CNT (15.1 %) relative to b-CNT that may be due to re-adsorption of CF_{6h} from suspension. The c-CNT show a considerable weight loss (7.3 %) compared to pristine CNT, however smaller than measured for the other oxidized CNT. The amount of CF_{6h} adsorbed by pristine CNT is almost six times larger than the amount adsorbed on b-CNT (formation of r-CNT), showing the ability of CF to establish π-π interactions with the pristine CNT. The weight loss also proceeds at slow rate from 150 ºC to 800 ºC, demonstrating the chemical similarity of the adsorbed CF_{6h} with the other oxidized materials. Considering the TGA weight loss observed for a-CNT, b-CNT, and the concentration of a-CNT in the suspensions prepared for alkaline treatment, the concentration of CF_{6h} formed after treatment is estimated to be approximately 0.8 mg L^{-1}. This value is consistent with the CF_{6h} concentration estimated from c-CNT weight loss, considering the concentration of pristine CNT in the CF_{6h} suspension used for treatment.

Structural characterization of CF

The CF were characterized by UV/Vis, fluorescence, FTIR, Raman and NMR spectroscopies. The UV/Vis spectra of CF, presented in Figure 3A, display a peak at low wavelength for all CF (≈300 nm). For CF_{6h} suspension, the absorption maximum is higher and a small peak appears at 560 nm. The color of CF suspensions depends on the refluxing time, tending to darker brown as oxidation time increases, indicating an increase of CF concentration (Figure 1).

Fluorescent spectra of CF suspensions displayed strong fluorescence emission at *ca.* 420 nm for an excitation wavelength of 290 nm (Figure 3B). CF suspensions obtained from higher refluxing time with acid, present an increase of fluorescence intensity as well as a shift of the emission peak to higher wavelength. The UV/Vis and fluorescence spectra of CF are similar to those reported in the literature for CF obtained by a similar experimental procedure.[32]This was interpreted by the authors as indicative of the presence of polycyclic aromatic hydrocarbons and conjugated double bonds, with extended oxygen containing functional groups.
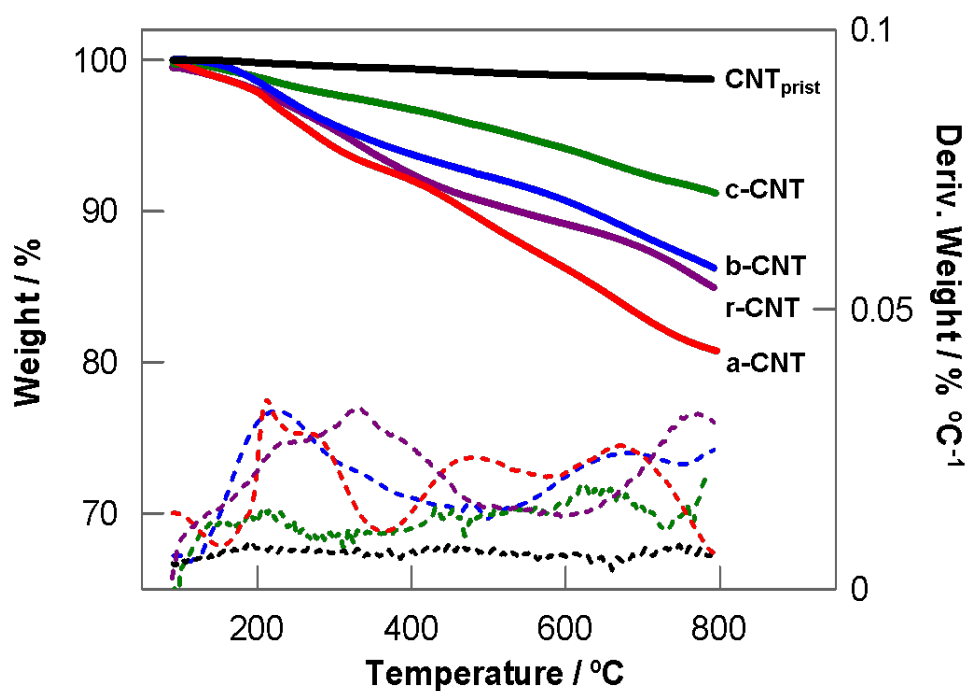
Figure 2. TGA curves and first derivative of CNT$_{prist}$, a-CNT, b-CNT, c-CNT and r-CNT.
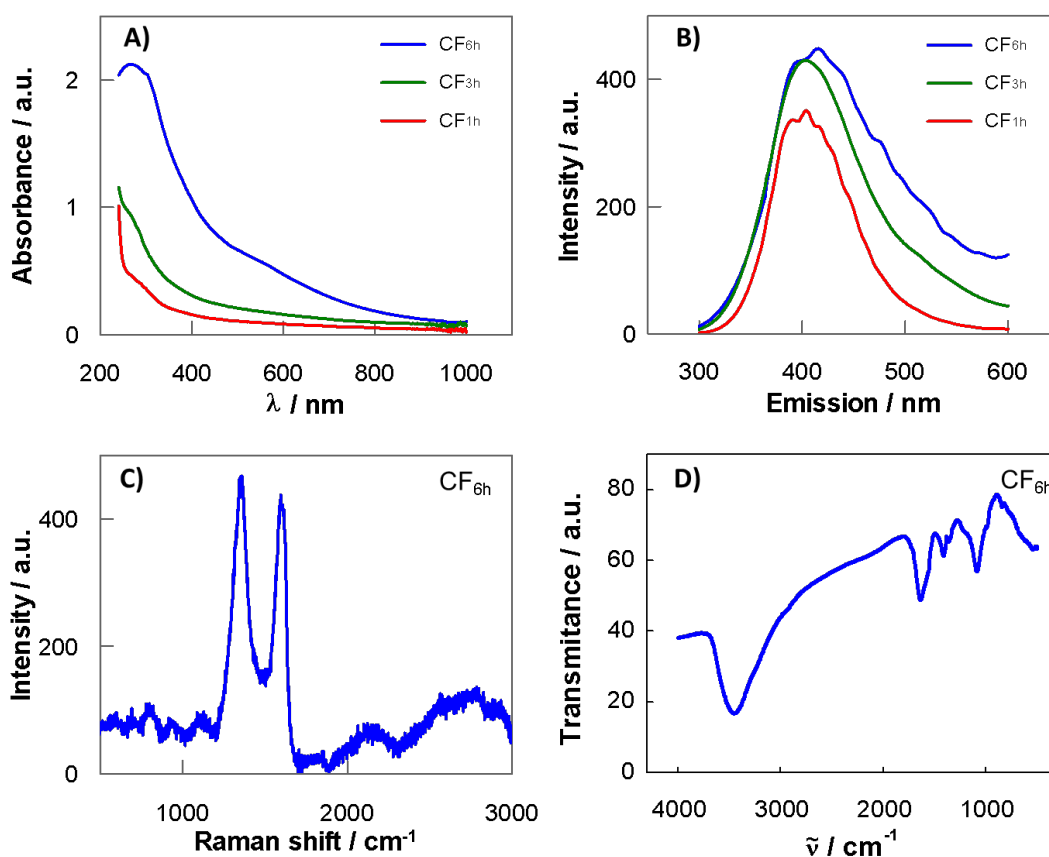

Figure 3. A) UV/Vis spectra of different CF; B) Fluorescence spectra of different CF; C) Raman spectrum of CF$_{6h}$; D) FTIR spectrum of CF$_{6h}$.

The FTIR spectrum (Figure 3D) confirms the presence of hydroxyl groups by an intense and broad signal at 3380 cm^{-1}, assigned to the stretching vibration of the O-H bond. Carbonyl groups in different chemical

environments can be associated to an equally broad signal spreading from 1695 to 1515 cm^{-1} and centered at 1615 cm^{-1}. This signal may indicate the presence of conjugated ketones, anhydrides, esters and/or lactones. The C=C stretching vibration usually leads to a low intensity signal in this region and the presence of this group can also be considered. The intense band at 1075 cm^{-1} can be due to the C-O stretching vibration in anhydrides, esters and carboxylic acids, supporting their presence in the CF$_{6h}$.

The Raman spectrum of CF$_{6h}$ is presented in Figure 3C, showing the characteristic G and D peaks of graphite and its derivatives. The G mode, observed in the range of 1500-1630 cm^{-1} has E$_{2g}$ symmetry, reflects the in-plane bond stretching motion of pairs of C sp^2 atoms.[45] This mode occurs at all sp^2 sites and does not require the presence of six-fold rings. The D mode, observed near 1350 cm^{-1}, is a breathing mode of A$_{1g}$ symmetry. This is a forbidden mode in perfect graphite, becoming active in the presence of disorder, indicating the existence of a hexagonal C sp^2 network disturbed by chemical bonding and formation of C sp^3 that reduces the network symmetry. [45] Raman spectra of CF$_{6h}$ were acquired across a large sample area for statistical analysis (Figure S1, supporting information) confirming that the CF$_{6h}$ material structure is based on hexagonal C sp^2 base-material with high disorder induced by chemical bonding, disturbing the perfect symmetry of the graphite structure. Finally, the 2D band typically detected near 2700 cm^{-1}, observed as a low intensity, wide band ranging from 2500-3000 cm^{-1}, which is characteristic of highly oxidized graphene-type of materials.[46]

STEM observation showed small carbonaceous fragments with tens to hundreds of microns of length (illustrative micrographs shown as supporting information). The elemental composition of CF was confirmed by EDS as mainly carbon and oxygen, with a considerable presence of NaCl resulting from the acid and alkaline treatments applied (supporting information).

The NMR data for the CF$_{6h}$ was recorded on a very dilute solution, requiring extensive accumulation of the signals in particular for the ^{13}C NMR spectrum. The use of deuterated water as solvent leads to rapid proton-deuterium exchange in the –OH unit of carboxylic acids and phenolic groups, preventing the visualization of these labile protons in the ^{1}H NMR spectrum. Protons bonded to carbon atoms are the only entities that can be identified in the spectrum.

The oxidizing conditions of the experiment may generate functional groups incorporating oxygen, namely hydroxyl, ketone, aldehyde or carboxylic acids. When some of these groups occupy adjacent positions in the molecular assembly, they can evolve to lactones or anhydrides. The formation of these groups was recently identified on the CNT surface, when alkenes were grafted onto CNT and oxidized by heating in sulfuric acid. The extensive formation of adipic anhydride was observed experimentally and theoretical calculations confirmed that this is a favored process either from the exposed alkene, from epoxides, vicinal diols or aldehydes, upon oxidation.[47]
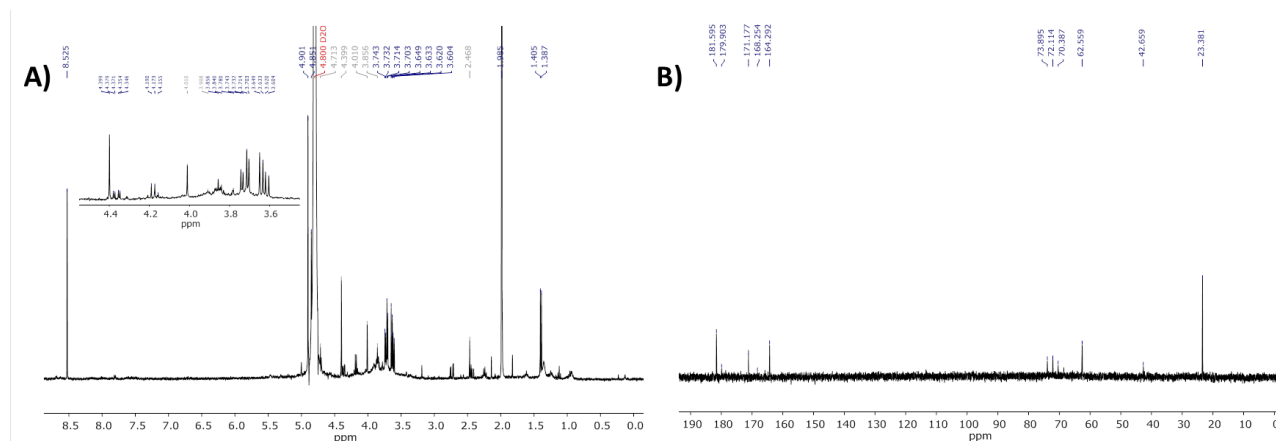
Figure 4. A) ^{1}H NMR (D$_2$O) of CF$_{6h}$; B) ^{13}C NMR (D$_2$O) of CF$_{6h}$.

Combining the experimental conditions with the ^{1}H NMR spectroscopic evidence (Figure 4A), we can identify a minute amount of equivalent aromatic protons (sharp singlet at δ 8.53 ppm) as most of the signals are generated by aliphatic protons (δ 1 – 4.5 ppm). The presence of signals in the δ 3.5 – 4.5 ppm region indicates that aliphatic protons are in the vicinity of electron-withdrawing hydroxyl groups and / or the oxygen atom of lactones. This assignment is supported by ^{13}C NMR (Figure 4B) that shows signals at δ 73.89, 72.11, 70.38 and 68.54 ppm, compatible with this type of substitution in slightly different chemical environments. The DEPT 135 experiment (in Figure S2) confirms that these signals correspond to a single proton linked to the sp^3 carbon. The same technique identifies the signal at δ 62.55 ppm as that of a CH$_2$ group, possibly linked to the oxygen atom of a lactone. The signal at δ 171.17 ppm can be assigned to the corresponding carbonyl group. Signals in the δ 1 – 3 ppm region correspond to more shielded aliphatic protons bonded to carbon atoms in the vicinity of carbonyl groups or inserted in a carbon chain or ring. The intense signal at δ 23.8 ppm in the ^{13}C NMR can also be assigned either to a methyl group or to a C-H carbon inserted in a carbon chain (by DEPT 135). The presence of carboxylic acids and / or anhydrides cannot be excluded as the intense signal at δ 164.29 ppm and the minor peak at δ 168.25 ppm are compatible with such carbonyl carbon atoms. The intense peak at δ 181.59 ppm and less intense peaks in its vicinity may be due to quinone-type carbonyl groups. The DEPT 135 technique confirms that none of these carbonyl groups is linked to a proton, confirming that the aldehyde function is either absent or is a negligible component in the CF$_{6h}$ material.

The role of CF on the voltammetric properties of CNT

The voltammetric characterization of the different CNT materials was performed after their immobilization at the surface of a GCE by drop casting and further evaporation of solvent, as described in the experimental section. The cyclic voltammograms acquired in PB solutions are displayed in Figure 5. The voltammograms obtained using unmodified GCE and CNT$_{prist}$@GCE display an almost flat profile with a residual current, while those from a-CNT, b-CNT, c-CNT and r-CNT exhibit a current response over the whole potential range. At the potential range from -0.5 V to 0 V, ascribed to the oxidation/ reduction of quinoid groups [48–50] only the voltammograms obtained from a-CNT@GCE and r-CNT@GCE display a significant current.

9

The voltammetry of HQ at CNT modified GCE provides important insight on the presence of oxo-surface groups. The possible interaction of C-OH groups (reduced form of HQ) and of C=O groups (oxidized form of HQ) with the oxo-surface groups may modify the voltammetric response of HQ. HQ is oxidized by a slow electron transfer process involving a two electron - two H^+ mechanism and its oxidized form can be reduced back.[22,51] The heterogeneous rate constant for HQ oxidation is quite sensitive to the interface structure and hence the voltammetric profile depends on the electrode nature.
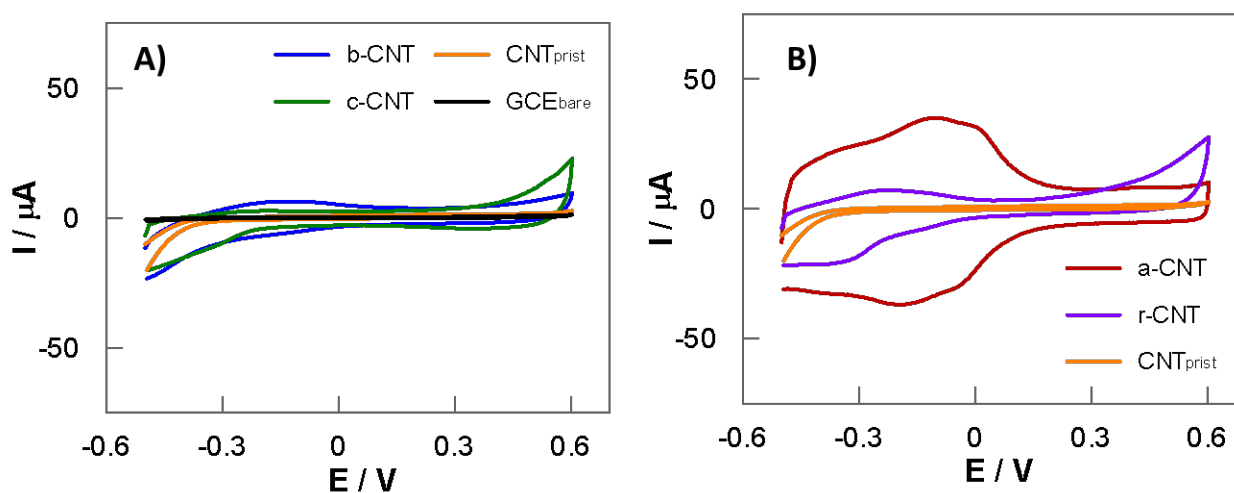

Figure 5. Voltammetric characterization of: A) unmodified GCE (GCE$_{bare}$) and GCE modified with b-CNT, c-CNT and CNT$_{prist}$; B) GCE modified with a-CNT, r-CNT and CNT$_{prist}$ in a PB pH 7.2 solution.

Voltammograms of HQ obtained with CNT$_{prist}$@GCE show an important potential shift of the anodic peak to less positive potentials with regard to voltammograms from GCE (Figure 6A). Deeper modifications are noticed when a-CNT@GCE is used, as in addition to the shift of the anodic peak, anodic and cathodic currents increase markedly (Figure 6B). This indicates that HQ interacts with the oxygen groups on the a-CNT surface. Furthermore, the increase of peaks current ratio, i_p^a / i_p^c, from 1.0 (for GCE and CNT$_{prist}$@GCE) to 1.6 (for a-CNT@GCE) (Table 1) suggests that the interactions are stronger with the reduced form of HQ than with the oxidized form. This result may be a consequence of the presence of quinoid units on a-CNT. The oxidation of these quinoid units at a potential lower than that of HQ leads to the conversion of phenolic groups to quinones. The consequent increase of C=O with respect to C-OH groups may enhance the interaction with the reduced form of HQ by hydrogen bonds.

In order to characterize the role of CF on the electrochemical behavior of oxidized CNT, voltammograms were recorded using b-CNT (prepared from a-CNT by reflux in NaOH solution), and c-CNT, (prepared from CNT$_{prist}$ that were in contact with CF suspension). Using either b-CNT@GCE or c-CNT@GCE the anodic and cathodic peaks of HQ are similar, displaying i_p^a / i_p^c close to 1.0 (Table 1).
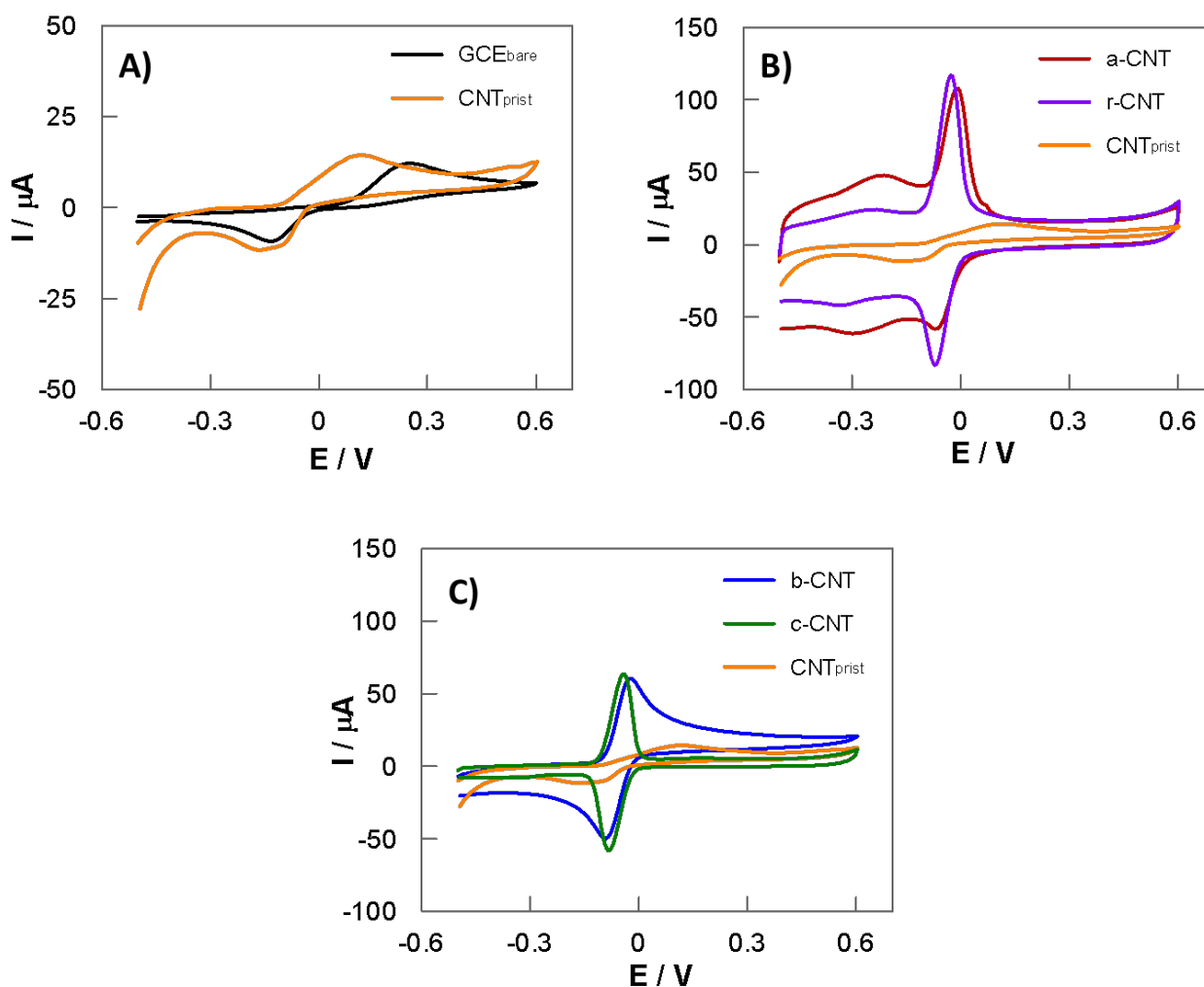
Figure 6. Voltammetric responses of 0.50 mM HQ in PB solution pH 7.2 using: A) bare GCE and CNT$_{prist}$@GCE; B) a-CNT@GCE, r-CNT@GCE and CNT$_{prist}$@GCE; C) b-CNT@GCE, c-CNT@GCE and CNT$_{prist}$@GCE.

Table 1. Characteristic parameters of the voltamogramms displayed in Figure 6.

Electrode	$\Delta E_p (E_p^a - E_p^c)$ (mV)	i_p^a / i_p^c	$E_p^a - (E_p^a)_{GCE}$ (mV)	$i_p^a / (i_p^a)_{GCE}$
GCE	389	1.0	0	1
CNT$_{prist}$@GCE	230	1.1	-144	1.3
a-CNT@GCE	64	1.6	-241	9.8
b-CNT@GCE	58	1.0	-286	7.4
c-CNT@GCE	44	1.1	-295	8.0
r-CNT@GCE	44	1.4	-280	10.9

The distinct voltammetric responses of c-CNT and r-CNT (obtained by adsorption of CF on CNT$_{prist}$ and b-CNT, respectively) indicate that the electrochemical behavior of CF is highly influenced by the interactions with the CNT surface. With the pristine CNT, the association is dominated by π-π interactions, with the polar groups of CF oriented towards the solution. The functionalization maintained on the b-CNT surface may be involved in polar and H-bond interactions with the extensively oxidized CF surface. In particular, the C-OH

and C=O groups of carboxylic acids may be involved in the generation of supramolecular arrangements. The presence of C-OH groups from CF and from b-CNT in neighboring positions may lead to molecular assemblies that mimic the electrochemical behavior of the quinoid units. The response pattern previously assigned to quinoid units in a-CNT (in the range of -0.5 to 0 V) is not evident in the voltammogram of b-CNT (Figure 5A and Figure 6C) and reappears on the voltammogram of r-CNT (Figure 5B and Figure 6B). The disruption and regeneration of these structures in an almost reversible manner reflects the labile nature of these supramolecular arrangements.

The response of HQ using r-CNT@GCE is different from the obtained with either b-CNT@GCE or c-CNT@GCE. The peaks asymmetry characterized by $i_p^a / i_p^c = 1.4$, although lower, resemble that observed for a-CNT@GCE ($i_p^a / i_p^c = 1.6$). Voltammograms from r-CNT also display the typical response of quinoid units previously described for a-CNT.

Another important feature associated to the presence of CF is its role on the adsorption of HQ. While voltammograms from a-CNT display a typical peak of an adsorption-controlled process (Figure 6B, a-CNT), voltammograms from b-CNT exhibit a shape typical of a diffusion-controlled process (Figure 6C, b-CNT). Voltammograms from c-CNT (Figure 6C, c-CNT) and from r-CNT (obtained by CF adsorbed on b-CNT) (Figure 6B, r-CNT) present the typical adsorption-controlled response. Thus, the CF present on a-CNT, c-CNT and r-CNT are likely to provide the active sites for adsorption of both reduced and oxidized forms of HQ. These evidences indicate that CF is an interesting material that can be used to tailor the surface of electrode to interact with specific molecules, facilitating the electron transfer process.

Voltammetric characterization of CF$_{6h}$ modified carbon electrodes

The suspension of CF$_{6h}$ (0.8 mg L^{-1}) was used to modify the surface of electrodes of different carbon materials, namely, SPCE, GCE, GCE coated with graphite powder (G$_{1\mu m}$@GCE) and GCE coated with carbon nanofibers (CNF@GCE). The voltammetric responses of HQ using these electrodes are displayed in Figure 7. As a general trend, the voltammetric curves show improved features when CF are drop casted on the electrodes surface. A marked shift of the peaks potential is visible, leading to the decrease of the ΔEp ($E_p^a - E_p^c$) and the shape of voltammograms becomes steeper (Table 2). These effects indicate that CF have important catalytic properties. For all electrodes an increase of current ranging from 30 to 180 % is observed depending on the micro / nano-structuration of the surface. The lower current increase, *ca.* 30 %, was observed for the smoother surface of glassy carbon, followed by the graphitic surfaces of SPCE and G$_{1\mu m}$@GCE, with a 60 % increase. The nanostructured surface of CNF@GCE, (CNF with 60-100 nm diameter), display a 180 % current increase. This trend is also observed c-CNT@GCE (Figure 6B). The CNT diameter is approximately 9.5 nm, and the measured current increases *ca.* 600 %, from CNT$_{prist}$ to c-CNT (Table 1). Besides, the shape of the voltammogram of CF-CNF@GCE deviates from a diffusion-controlled to an adsorption-controlled process, as previously remarked for c-CNT.
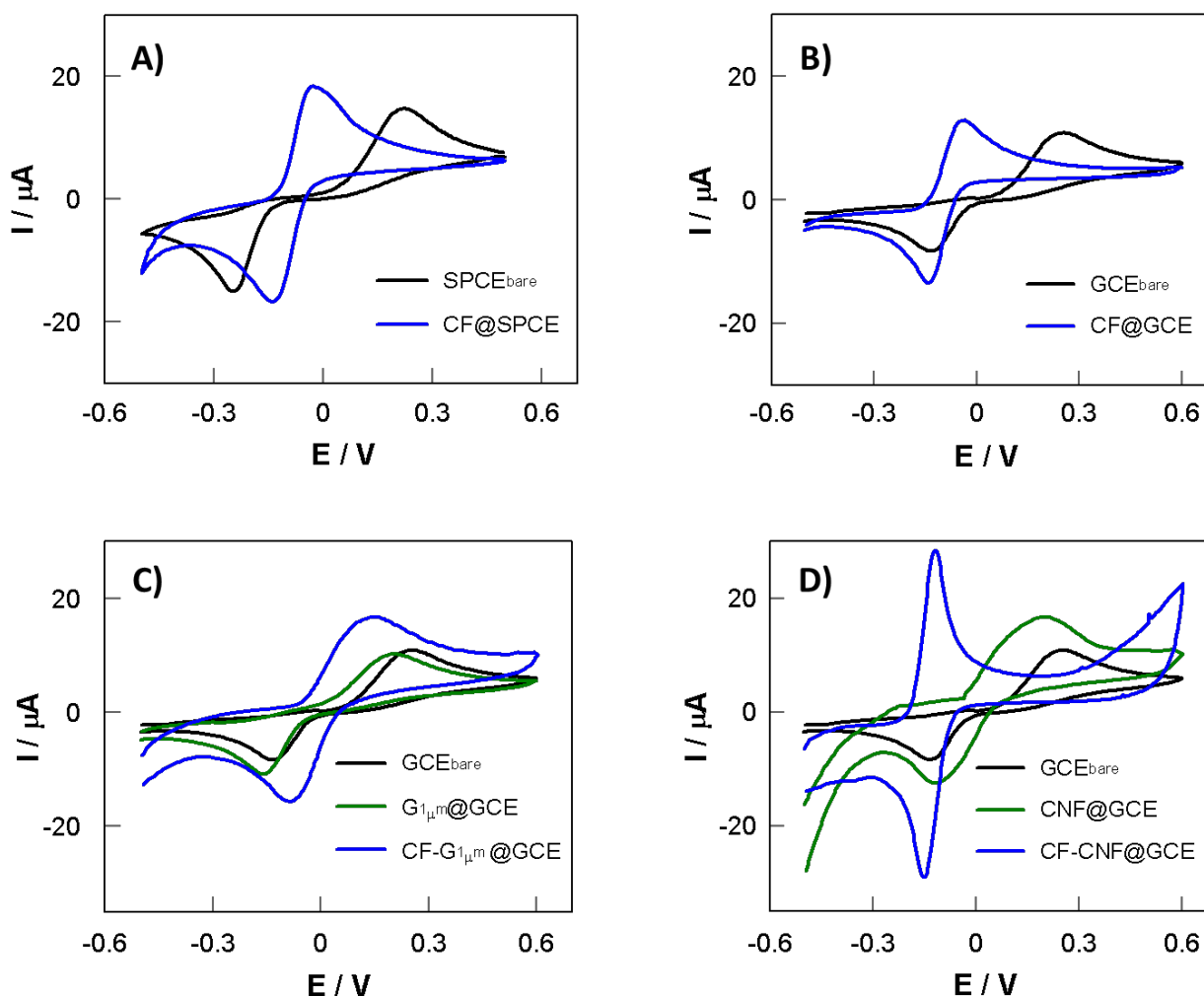
Figure 7. Voltammetric characterization of different carbon electrodes modified with CF_{6h} obtained in a 0.50 mM of HQ, 0.15 M PB pH 7.2. A) SPCE; B) GCE; C) $G_{1\mu m}$@GCE and D) CNF@GCE.

Table 2. Characteristic parameters of the voltamogramms displayed in Figure 7.

Electrode	$\Delta E_p (E_p^a - E_p^c)$ (mV)		$(E_p^a)_{with\ CF} - (E_p^a)_{without\ CF}$ (mV)	i_p^a / i_p^c		$(i_p^a)_{with\ CF} / (i_p^a)_{without\ CF}$
	without CF	with CF		without CF	with CF	
SPCE	459	103	-244	0.9	1.1	1.6
GCE	389	83	-300	1.0	0.9	1.3
$G_{1\mu m}$@GCE	342	215	-127	0.9	0.9	1.6
CNF@GCE	273	29	-288	0.9	1.2	2.8

4. Conclusion

The CF obtained by oxidation of CNT were characterized by spectroscopic techniques and visualized by STEM. Fluorescence and Raman spectroscopies indicate the presence of alkenes and graphene-type conjugated aromatic rings, with highly oxidized moieties. The presence of alcohols and carbonyl groups,

some of them associated to aliphatic fragments and probably incorporated as phenols, quinones, lactones, anhydrides and carboxylic acids, is supported by FTIR and NMR spectroscopy.

Our results demonstrate that CF have the ability to strongly adsorb on carbon-based surfaces with different functionalization level. CF adsorbs on CNT_{prist} and on oxidized CNT (b-CNT) yielding c-CNT and r-CNT, respectively. These CNT materials displayed dissimilar voltammetric response demonstrating that the interaction between CF and the CNT surface, as well as the chemistry of the underlying CNT surface, play a fundamental role on the voltammetric response of these materials.

The CF-modified CNT revealed important electrocatalytic effects observed by changes in the shape of HQ voltammograms, potential shifts, and current increase. The electrodes that were modified with CF-containing CNT, namely a-CNT, c-CNT and r-CNT, display a voltammetric response for HQ typical of adsorption-controlled processes, while electrodes modified with b-CNT (prepared by removing CF from a-CNT) display a typical diffusion-controlled response. Therefore, the active sites for HQ adsorption strongly correlate with the presence of CF.

Our results indicate that the voltammetric behavior of CF is highly influenced by their interaction with CNT surface. The CF association with the pristine CNT may be dominated by π-π interactions, while with oxidized CNT it may involve polar and H-bond interactions. In particular, the strong H-bond involving C-OH and C=O groups of carboxylic acids generate supramolecular arrangements that mimic the electrochemical response of quinoid units. The disruption (by alkali treatment of a-CNT) and regeneration (by adsorption of CF on b-CNT) of these structures in an almost reversible manner reflects the labile nature of these supramolecular arrangements.

In voltammetric experiment these quinoid units on the CNT surface are oxidized, decreasing the concentration of C-OH groups by conversion to C=O groups. The more extensive interaction of the reduced form of HQ with the electrochemically oxidized electrode surface is demonstrated by the higher anodic relative to the cathodic peak.

The use of CF for the functionalization of carbon electrodes was evaluated for the detection of HQ as a model polyphenol. Voltammograms from modified glassy carbon, graphite and carbon nanofiber electrodes exhibited improved responses with regard to HQ oxidation. The magnitude of the effects depended strongly on the electrode surface roughness, the rougher surfaces presenting the higher effects.

Acknowledgements

Figure 1. Schematic illustration of: the CNT treatments carried out for the preparation of carbonaceous fragments suspensions (CF); the functionalization of different CNT and of the surface of carbon electrodes with CF_{6h}. CNT_{prist}: pristine CNT; a-CNT: CNT oxidized in HNO_3 reflux; b-CNT: obtained by treatment of a-CNT with 0.1 M NaOH, 1 h of reflux; c-CNT: CNT_{prist} mechanically stirred in CF_{6h} suspension; r-CNT: b-CNT mechanically stirred in CF_{6h} suspension. $CF-G_{1\mu m}@GCE$: GCE coated with graphite powder and modified with CF_{6h}; CF-CNF@GCE: GCE coated with carbon nanofibers and modified with CF_{6h}; CF@GCE: GCE modified with CF_{6h}; CF@SPCE: SPCE modified with CF_{6h}.

Figure 2. TGA curves and first derivative of CNT_{prist}, a-CNT, b-CNT, c-CNT and r-CNT.

Figure 3. A) UV/Vis spectra of different CF; B) Fluorescence spectra of different CF; C) Raman spectrum of CF_{6h}; D) FTIR spectrum of CF_{6h}.

Figure 4. A) ^1H NMR (D_2O) of CF_{6h}; B) ^{13}C NMR (D_2O) of $CF_{6h.}$

Figure 5. Voltammetric characterization of: A) unmodified GCE (GCE_{bare}) and GCE modified with b-CNT, c-CNT and CNT_{prist}; B) GCE modified with a-CNT, r-CNT and CNT_{prist} in a PB pH 7.2 solution.

Figure 6. Voltammetric responses of 0.50 mM HQ in PB solution pH 7.2 using: A) bare GCE and $CNT_{prist}@GCE$; B) a-CNT@GCE, r-CNT@GCE and $CNT_{prist}@GCE$; C) b-CNT@GCE, c-CNT@GCE and $CNT_{prist}@GCE$.

Figure 7. Voltammetric characterization of different carbon electrodes modified with CF_{6h} obtained in a 0.50 mM of HQ, 0.15 M PB pH 7.2. A) SPCE; B) GCE; C) $G_{1\mu m}@GCE$ and D) CNF@GCE.

5. References

[1]   W. Zhang, S. Zhu, R. Luque, S. Han, L. Hu, G. Xu, *Chem. Soc. Rev.* **2016**, *45*, 715–752.

[2]   S. Marchesan, M. Melchionna, M. Prato, *ACS Nano* **2015**, *9*, 9441–9450.

[3]   A. Ambrosi, C. K. Chua, N. M. Latiff, A. H. Loo, C. H. A. Wong, A. Y. S. Eng, A. Bonanni, M. Pumera, *Chem. Soc. Rev.* **2016**, *45*, 2458–2493.

[4]   A. Martín, A. Escarpa, *TrAC Trends Anal. Chem.* **2014**, *56*, 13–26.

[5]   W. Gao, Y. Wan, Y. Dou, D. Zhao, *Adv. Energy Mater.* **2011**, *1*, 115–123.

[6]   C. E. Banks, R. G. Compton, *Analyst* **2006**, *131*, 15–21.

[7]   C. E. Banks, A. Crossley, C. Salter, S. J. Wilkins, R. G. Compton, *Angew. Chemie - Int. Ed.* **2006**, *45*, 2533–2537.

[8]   M. C. Henstridge, L. Shao, G. G. Wildgoose, R. G. Compton, G. Tobias, M. L. H. Green, *Electroanalysis* **2008**, *20*, 498–506.

[9]   X. Chia, A. Ambrosi, M. Pumera, *Electrochem. Commun.* **2014**, *38*, 1–3.

[10]   L. Wang, A. Ambrosi, M. Pumera, *Electrochem. Commun.* **2013**, *26*, 71–73.

[11]   L. Wang, A. Ambrosi, M. Pumera, *Anal. Chem.* **2013**, *85*, 6195–6197.

[12]   A. Ambrosi, M. Pumera, *Chem. - A Eur. J.* **2010**, *16*, 10946–10949.

[13]   A. Ambrosi, M. Pumera, *J. Phys. Chem. C* **2011**, *115*, 25281–25284.

[14]   E. L. K. Chng, M. Pumera, *Chem. - A Eur. J.* **2012**, *18*, 1401–1407.

[15]   D. A. C. Brownson, C. E. Banks, *Electrochem. Commun.* **2011**, *13*, 111–113.

[16]   R. Gusmão, Z. Sofer, M. Novacek, J. Luxa, S. Matejkova, M. Pumera, *Nanoscale* **2016**, *8*, 6700–6711.

[17]   D. V Kosynkin, A. L. Higginbotham, A. Sinitskii, J. R. Lomeda, A. Dimiev, B. K. Price, J. M. Tour, *Nature* **2009**, *458*, 872–876.

[18]   W. S. Hummers, R. E. Offeman, *J. Am. Chem. Soc.* **1958**, *80*, 1339–1339.

[19]   M. N. Tchoul, W. T. Ford, G. Lolli, D. E. Resasco, S. Arepalli, *Chem. Mater.* **2007**, *19*, 5765–5772.

[20]   I. D. Rosca, F. Watari, M. Uo, T. Akasaka, *Carbon N. Y.* **2005**, *43*, 3124–3131.

[21]   M. Thiruppathi, N. Thiyagarajan, M. Gopinathan, J.-M. Zen, *Electrochem. Commun.* **2016**, *69*, 15–18.

[22]   R. Gusmão, V. López-Puente, I. Pastoriza-Santos, J. Pérez-Juste, M. F. Proença, F. Bento, D. Geraldo, M. C. Paiva, E. Gonzalez-Romero, *RSC Adv.* **2015**, *5*, 5024–5031.

[23]   K. Jurkschat, X. Ji, A. Crossley, R. G. Compton, C. E. Banks, *Analyst* **2007**, *132*, 21–23.

[24]   H. Hu, B. Zhao, M. E. Itkis, R. C. Haddon, *J. Phys. Chem. B* **2003**, *107*, 13838–13842.

[25]   U. Anik, S. Cevik, M. Pumera, *Nanoscale Res. Lett.* **2010**, *5*, 846–852.

[26]   A. Ambrosi, C. K. Chua, B. Khezri, Z. Sofer, R. D. Webster, M. Pumera, *Proc. Natl. Acad. Sci.* **2012**, *109*, 12899–12904.

[27]   S. Fogden, R. Verdejo, B. Cottam, M. Shaffer, *Chem. Phys. Lett.* **2008**, *460*, 162–167.

[28]   J. P. Rourke, P. A. Pandey, J. J. Moore, M. Bates, I. A. Kinloch, R. J. Young, N. R. Wilson, *Angew. Chemie - Int. Ed.* **2011**, *50*, 3173–3177.

[29]   R. Verdejo, S. Lamoriniere, B. Cottam, A. Bismarck, M. Shaffer, *Chem. Commun.* **2007**, 513–515.

[30]   C. G. Salzmann, S. A. Llewellyn, G. Tobias, M. A. H. Ward, Y. Huh, M. L. H. Green, *Adv. Mater.* **2007**, *19*, 883–887.

[31]   K. A. Worsley, R. W. Kondrat, S. K. Pal, I. Kalinina, R. C. Haddon, *Carbon N. Y.* **2011**, *49*, 4982–4986.

[32]   X. Ma, L. Jia, L. Zhang, L. Zhu, *Chem. - Eur. J.* **2014**, *20*, 4072–4076.

[33]   D. Ma, L. Dong, M. Zhou, L. Zhu, *Analyst* **2016**, 2761–2766.

[34]   X. Li, X. Yang, L. Jia, X. Ma, L. Zhu, *Electrochem. Commun.* **2012**, *23*, 94–97.

[35]   X. Li, D. Ma, L. Zhu, *Chem. - A Eur. J.* **2015**, *21*, 17239–17244.

[36]   X. Yang, X. Li, X. Ma, L. Jia, L. Zhu, *RSC Adv.* **2013**, *3*, 6752–6755.

[37]   X. Yang, X. Li, X. Ma, L. Jia, L. Zhu, *Electroanalysis* **2014**, *26*, 139–146.

[38]   A. Bonanni, A. Ambrosi, C. K. Chua, M. Pumera, *ACS Nano* **2014**, *8*, 4197–4204.

[39]   L. Wang, A. Ambrosi, M. Pumera, *Chem. - An Asian J.* **2013**, *8*, 1200–1204.

[40]   D. Stéfani, A. J. Paula, B. G. Vaz, R. A. Silva, N. F. Andrade, G. Z. Justo, C. V Ferreira, A. G. S. Filho, M. N. Eberlin, O. L. Alves, *J. Hazard. Mater.* **2011**, *189*, 391–396.

[41]   J. Zhong, T. Xie, J. Deng, X. Sun, X. Pan, X. Bao, Z. Wu, *Chem. Commun.* **2011**, *47*, 8373–8375.

[42]   G. Busca, S. Berardinelli, C. Resini, L. Arrighi, *J. Hazard. Mater.* **2008**, *160*, 265–288.

[43]   K. B. Pandey, S. I. Rizvi, *Oxid. Med. Cell. Longev.* **2009**, *2*, 270–278.

[44]   C. A. Rice-Evans, N. J. Miller, G. Paganga, *Free Radic. Biol. Med.* **1996**, *20*, 933–956.

[45]   A. C. Ferrari, J. Robertson, *Phys. Rev. B* **2000**, *61*, 14095–14107.

[46]   D. Yang, A. Velamakanni, G. Bozoklu, S. Park, M. Stoller, R. D. Piner, S. Stankovich, I. Jung, D. A.

Field, C. A. Ventrice Jr., R. S. Ruoff, *Carbon N. Y.* **2009**, *47*, 145–152.

[47]   R. F. Araújo, M. F. Proença, C. J. Silva, T. G. Castro, M. Melle-Franco, M. C. Paiva, S. Villar-Rodil, J. M. D. Tascón, *Carbon N. Y.* **2016**, *98*, 421–431.

[48]   Y. Xing, L. Li, C. C. Chusuei, R. V Hull, *Langmuir* **2005**, *21*, 4185–4190.

[49]   R. Gusmão, M. Melle-Franco, D. Geraldo, F. Bento, F. Proença, M. C. Paiva, *Electrochem. Commun.* **2015**, *57*, 22–26.

[50]   C. A. Thorogood, G. G. Wildgoose, A. Crossley, R. M. J. Jacobs, J. H. Jones, R. G. Compton, *Chem. Mater.* **2007**, *19*, 4964–4974.

[51]   P. T. Lee, J. C. Harfield, A. Crossley, B. S. Pilgrim, R. G. Compton, *RSC Adv.* **2013**, *3*, 7347–7354.